

The droplet size distribution and its dynamics in chemically active emulsions

Jonathan Bauermann,^{1,*} Giacomo Bartolucci,² Christoph A. Weber,³ and Frank Jülicher^{4,5,6,†}

¹*Department of Physics, Harvard University, Cambridge, MA 02138, USA*

²*Department of Physics, Universitat de Barcelona, Barcelona, Spain*

³*Faculty of Mathematics, Natural Sciences, and Materials Engineering,
Institute of Physics, University of Augsburg, Augsburg, Germany*

⁴*Max Planck Institute for the Physics of Complex Systems, Dresden, Germany*

⁵*Center for Systems Biology Dresden, Dresden, Germany*

⁶*Cluster of Excellence Physics of Life, TU Dresden, 01062 Dresden, Germany*

(Dated: January 28, 2025)

We present a dynamic theory for the droplet size distribution in chemically active emulsions, considering a simple ternary mixture with a conserved density. We show that the collective behavior of many droplets, such as monodispersity, emerges through a coupling of the conserved density in the far field. Using our theory, we determine the stationary state of such emulsions and characterize the relaxation of the droplet size distributions at late times. A key finding is a universal scaling behavior, leading to the collapse of the rescaled size distributions at late times. Our results suggest that the key features of our dynamic theory are generic and apply to the broader class of multi-component systems with conservation laws and active chemical reactions.

Domain ripening is a hallmark of the dynamics of phase-separated systems such as emulsions that undergo liquid-liquid phase separation or liquids undergoing crystallization [1–5]. In such processes, larger domains of a new phase grow at the expense of smaller ones that shrink and eventually dissolve, allowing the system to approach thermodynamic equilibrium. The seminal work of Lifshitz, Slyozov, and Wagner revealed that in three-dimensional systems, the average droplet size scales with $\langle R \rangle(t) \propto t^{1/3}$ and the number of droplets decreases as $N(t) \propto t^{-1}$ [6, 7]. Furthermore, in the late stages of ripening, they reported a universal shape of the droplet size distribution that is independent of the physical parameters and time.

In active systems, the droplet dynamics can vastly differ. Ultimately, ripening can even be reversed when the system is actively maintained away from equilibrium [8–13]. A particular exciting class of such systems are chemically active emulsions, where chemical reactions are maintained away from equilibrium [14–17]. The physical setting of phase separation and non-equilibrium chemical reactions is relevant for cell biology with a growing number of studies of biomolecular condensates in living cells [18–22]. Chemically active emulsions have gained a lot of interest in recent years with experimental biophysical [23, 24] and chemical systems [25–28], as well as theoretical studies [11, 16, 29–35]. The suppression of ripening in binary active emulsions relies on a simple mechanism [8, 9]: When the components enriched in the droplet are actively degraded inside or produced outside of the droplet, a stationary droplet radius exists for which diffusive fluxes balance the chemical fluxes. However, in multi-component mixtures, the quantities conserved by the reaction also determine together with the chemical fluxes whether single droplets can adopt a stationary radius or grow like passive droplets [36]. Here, we pro-

pose a dynamic theory for a chemically active emulsion that is minimal in terms of its components and, thereby, amenable to the methods developed by Lifshitz, Slyozov, Wagner, and others for binary emulsions without chemical reactions [6, 7, 37, 38].

Theory of ripening of a chemically active emulsion - This theory involves both conserved densities and active chemical reactions. A minimal scenario is a ternary mixture with only one chemical reaction. We therefore consider three components A , B , and S and the monomolecular reaction $A \rightleftharpoons B$. The dynamics of the concentration fields c_i with $i = A, B$ can be written as $\partial_t c_i = \Gamma_i \nabla^2 \mu_i - k_{ji} c_i + k_{ij} c_j$, where Γ_i denote mobility coefficients, and μ_i are the chemical potentials that be determined from the system's free energy. The reaction rate coefficients k_{ij} specify the reaction kinetics and determine whether the system is active or passive. For passive systems, the reaction rate coefficients k_{ij} are constrained such that $k_{ABC} = k_{BCA}$ when $\mu_A = \mu_B$, leading to a unique thermodynamic equilibrium. This property is illustrated in the ternary phase diagrams of a passive mixture (Fig. 1(a)). Whenever the reaction nullcline (yellow) intersects the binodal of the ternary system without reactions, these intersection points are connected by a tie-line, allowing for a thermodynamic equilibrium of phases and chemical reactions. Systems for which the reaction rate coefficients k_{ij} do not obey this relation, are chemically active. This is the case e.g. if k_{ij} are chosen constant in the example of Fig. 1(c). Here, the resulting reaction nullcline (red) intersects the binodal at two points not connected by a tie-line, and the system cannot relax to a thermodynamic equilibrium [39].

The coexistence of phases is governed by the quantity $\psi = (c_A + c_B)/2$ that is conserved by the chemical reaction, both in the passive and the active case. We illustrate this property in Fig. 1 with three different lines of

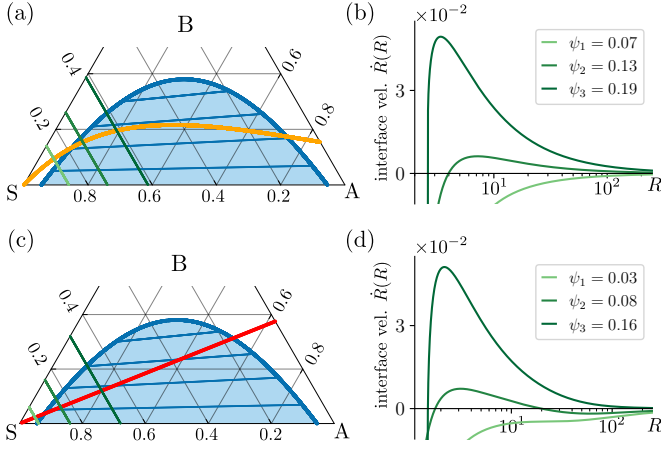


FIG. 1. **Passive and active emulsion.** (a,c): phase diagram of ternary emulsions with passive or active chemical reaction $A \rightleftharpoons B$. The binodal (thick blue), tie-lines (thin blue), and the reaction nullcline for passive (yellow) and active (red) reactions are shown. Lines of constant $\psi = 0.07, 0.13, 0.19$ (a) and $\psi = 0.03, 0.08, 0.16$ (b) are highlighted (green). (b,d): Interface velocities \dot{R} as a function of radius R for single droplets are shown for these values of ψ . Phase diagram and interface velocities were obtained using a Flory-Huggins mean field model of mixtures; see the App. for details

constant ψ shown in green in the phase diagrams for each case. The line of the smallest value of the conserved quantity ψ (brightest green) intersects the reaction nullcline outside the binodal domains leading to a homogeneous steady state with vanishing reaction fluxes. However, for larger values of ψ (darker green shades), this intersection lies within the binodal domain. Thus, two phases coexist. For the passive case, there is a unique thermodynamic equilibrium state for which the coexisting phases and the chemical reactions are at equilibrium. A passive emulsion of droplets will undergo ripening, relaxing toward this thermodynamic equilibrium state. However, the behavior on long-time scales of an active emulsion is unclear since thermodynamic equilibrium cannot act as a global attractor of the ripening dynamics. To derive the dynamics of such an active emulsion, we express the dynamics of the conserved quantity $\psi = (c_A + c_B)/2$, together with the dynamics of the non-conserved quantity $\xi = (c_A - c_B)/2$, the extent of reaction, as

$$\partial_t \psi = \Gamma \nabla^2 \mu_\psi, \quad \partial_t \xi = \Gamma \nabla^2 \mu_\xi - K \xi + \mathcal{S} \psi, \quad (1)$$

where $K = k_{AB} + k_{BA}$, $\mathcal{S} = k_{AB} - k_{BA}$. We chose the same mobility $\Gamma = \Gamma_i$ for both components, for simplicity, and defined $\mu_\psi = (\mu_A + \mu_B)/2$ and $\mu_\xi = (\mu_A - \mu_B)/2$ as the corresponding chemical potentials of ψ and ξ .

In the following, we first discuss the single droplet dynamics in a quasistationary limit and then derive the collective dynamics of many droplets via coupling the far-field concentration via a conservation law similar to the method developed by Lifshitz, Slyosov, Wagner and

others for the ripening of passive emulsions [6, 7, 37, 38]. After showing examples of such active emulsions, we derive the stationary limit of the active emulsion and show the scaling behavior in the late-time regime.

Single droplet dynamics - We derive the slow interface dynamics in a quasistationary limit. To this aim, we determine the stationary solutions of the dynamical Eqs. (1) for one single droplet of radius R located at the origin of the coordinate system. Specifically, we expand Eq. (1) up to linear order on both sides, inside ($r < R$) and outside ($r > R$), around the respective values of concentrations at the interface, leading to

$$\partial_t \psi = D_\psi^{i/o} \nabla^2 \psi, \quad \partial_t \xi = D_\xi^{i/o} \nabla^2 \xi - k^{i/o} \xi + s^{i/o} \psi, \quad (2)$$

where D_ψ , D_ξ , k and s denote the kinetic coefficients and the upper indices i/o denote the inside/outside domain, respectively [30]. The stationary field for the conserved quantity is given by

$$\psi^i = \Psi_R^i, \quad \psi^o(r) = \Psi^\infty + \frac{R(\Psi_R^o - \Psi^\infty)}{r}, \quad (3)$$

where $\Psi_R^{i/o}$ denote the concentrations of ψ at the interface and Ψ^∞ the value far from the droplet. For the non-conserved field, we find

$$\begin{aligned} \xi^i(r) &= \frac{s^i \Psi_R^i}{k^i} + \left(\Xi_R^i - \frac{s^i \Psi_R^i}{k^i} \right) \frac{i_0(\lambda^i r)}{i_0^i(\lambda^i R)}, \\ \xi^o(r) &= \frac{s^o \Psi^\infty}{k^o} + \frac{s^o R (\Psi_R^o - \Psi^\infty)}{k^o r} \\ &\quad + \left(\Xi_R^o - \frac{s^o \Psi_R^o}{k^o} \right) \frac{k_0(\lambda^o r)}{k_0(\lambda^o R)}. \end{aligned} \quad (4a)$$

Similarly, $\Xi_R^{i/o}$ denote the concentrations of ξ at both sides of the interface, $i_0(x) = \sinh(x)/x$, and $k_0^o(x) = \exp(-x)/x$ are the modified spherical Bessel function of the first and second kind and zeroth order. Furthermore, we have introduced the inverse reaction-diffusion length scale $\lambda^{i/o} = \sqrt{k^{i/o}/D_\xi^{i/o}}$.

We now derive the conditions for the interface concentrations. In contrast to binary mixtures, interface concentrations in a ternary mixture are not uniquely fixed. For a slow-moving interface, we impose that phase equilibrium is satisfied locally. Taking the Laplace pressure of a spherical droplet into account, these conditions read [40]

$$\begin{aligned} \mu_\psi^i &= \mu_\psi^o, \quad \mu_\xi^i = \mu_\xi^o, \\ f^i - f^o &= \mu_\psi^{i/o} (\Psi_R^i - \Psi_R^o) + \mu_\psi^{i/o} (\Xi_R^i - \Xi_R^o) - \frac{2\gamma}{R}, \end{aligned} \quad (5a)$$

where $f^{i/o}$ is the free energy density evaluated in the corresponding phase and $\mu_n^{i/o} = \partial f^{i/o} / \partial n$, with $n = \psi, \xi$, are

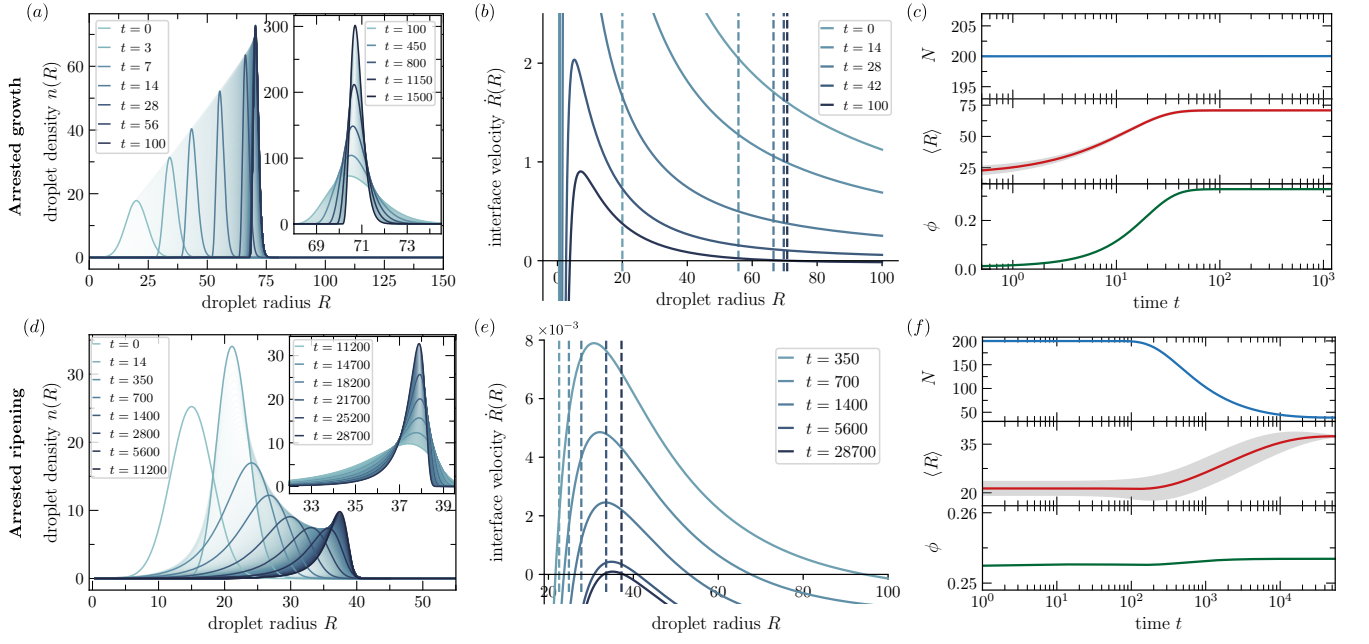


FIG. 2. **Dynamics of droplet size distributions in chemically active emulsions.** (a) Distribution $n(R)$ of droplet sizes for different times t for an arrested growth scenario (thick blue lines). The shading indicates distributions at intermediate times, revealing the arrest in a monodisperse distribution at late times. The inset shows late-time distributions. (b) Interface velocities $\dot{R}(R)$ for selected time points. The average radii at different times are indicated (dashed vertical lines) (c) Droplet number N , average radius $\langle R \rangle$, and the phase fraction ϕ as a function of time. (d-f) Same plots as (a-c) but for a scenario of arrested ripening. Parameters: Initial droplet number $N = 200$ in reference volume V_{ref} , Gaussian initial distribution $\mathcal{N}(\bar{R}_0, \sigma_R)$, $b = 1$, $c_0 = 1$, $D_{\psi}^{i/o} = 1$, $\gamma = 1/6$, $V_{\text{ref}} = 4\pi R_{\text{ref}}^3/3$, $R_{\text{ref}} = 600$, $k_{AB}^{i/o}/k_{BA}^{i/o} = 2.5$; arrested growth: $\alpha = 0.15\pi$, $\Psi_{\text{tot}} = -0.5$, $k_{AB}^{i/o} = 0.0013$, $\bar{R}_0 = 20$, $\sigma_R = 20$, arrested ripening: $\alpha = 0.23\pi$, $\Psi_{\text{tot}} = -0.7$, $k_{AB}^{i/o} = 0.0009$, $\bar{R}_0 = 15$, $\sigma_R = 10$.

the corresponding chemical potentials. Similar to ripening in ternary passive mixtures [41], the final interface condition follows from local material conservation:

$$\frac{j_{\psi}^i(R) - j_{\psi}^o(R)}{\Psi_R^i - \Psi_R^o} = \frac{j_{\xi}^i(R) - j_{\xi}^o(R)}{\Xi_R^i - \Xi_R^o}, \quad (6)$$

where the flux densities in the radial direction defined are $j_{\psi}^{i/o}(R) = -D_{\psi}^{i/o} \partial_r \psi^{i/o}(R)$ and $j_{\xi}^{i/o}(R) = -D_{\xi}^{i/o} \partial_r \xi^{i/o}(R)$. With these boundary conditions, all four interface concentrations are uniquely defined, and we can solve for the interface concentrations of the conserved quantity, $\Psi_R^{i/o} = \Psi_R^{i/o}(R, \Psi^{\infty})$, and non-conserved quantity $\Xi_R^{i/o} = \Xi_R^{i/o}(R, \Psi^{\infty})$. Furthermore, the same local material conservation law at the interface sets its velocity $\dot{R} = (j_{\psi}^i(R) - j_{\psi}^o(R)) / (\Psi_R^i - \Psi_R^o)$ [42]. Thus, we find

$$\dot{R}(R, \Psi^{\infty}) = \frac{D_{\psi}^o}{R} \frac{\Psi^{\infty} - \Psi_R^o(R, \Psi^{\infty})}{\Psi_R^i(R, \Psi^{\infty}) - \Psi_R^o(R, \Psi^{\infty})}. \quad (7)$$

We have explicitly stated that the equilibrium values $\Psi_R^{i/o}$ depend on both the droplet radius R and the far-field concentration Ψ^{∞} , in contrast to the simple case of binary mixtures where it only depends on R .

In Fig. 1(b,d), we show \dot{R} as a function of radius R for a single droplet for passive and active cases. For conserved quantities that intersect the reaction nullcline within the binodal region (cases of ψ_2 and ψ_3 in Fig. 1), there exists one unstable root of the interface velocity, known as the critical nucleation radius. For passive systems, the interface velocity stays positive for larger droplets, and a single droplet larger than this radius continuously grows. For active systems, however, there is a range of conserved quantities where a second root of the \dot{R} -curve exits, which is stable. This case corresponds to intensive droplets; see for example ψ_2 in Fig. 1(d). However, the ψ -range with intensive droplets is finite. At a critical value of the conserved quantity $\psi = \psi_{\text{crit}}$, the stable root diverges. Beyond this critical transition, single droplets grow limitless, and are thus referred to as extensive droplets [36].

Emulsion dynamics - Following the approach developed for Ostwald ripening [6, 7, 37, 38], we introduce the droplet size distribution $n(R)$. After droplets have nucleated, the initial distribution evolves in time according to a conserved dynamics:

$$\partial_t n = -\partial_R(n\dot{R}). \quad (8)$$

The disappearance of droplets at $R = 0$ is reflected by the boundary condition $n(R = 0, t) = 0$ for all times t .

With the help of this distribution $n(R, t)$, we define the phase fraction

$$\phi(t) = \frac{4\pi}{3V_{\text{ref}}} \int_0^\infty dR R^3 n(R, t), \quad (9)$$

which denotes the fraction of volume occupied by $N(t) = \int_0^\infty dR n(R, t)$ droplets in the reference volume V_{ref} at time t . The average droplet radius is

$$\langle R(t) \rangle = \frac{1}{N(t)} \int_0^\infty dR R n(R, t). \quad (10)$$

Finally, we have to invoke the overall conservation of the conserved material ψ in our system. We write as a mean-field approximation

$$\Psi_{\text{tot}} = \phi(t) \Psi_R^i(\langle R(t) \rangle, \Psi^\infty(t)) + (1 - \phi(t)) \Psi^\infty(t), \quad (11)$$

where Ψ_{tot} is the overall conserved concentration of ψ in our reference system, which is fixed and serves as a control parameter.

These equations provide a closed dynamics for the droplet size distribution. Explicitly, once we know the size distribution of droplets $n(R, t_0)$ at time t_0 , we use Eq. (9) and Eq. (10) to determine $\phi(t_0)$ and $\langle R(t_0) \rangle$. Equation (11) then uniquely specifies the concentration Ψ^∞ , and thus the interface velocity \dot{R} for any radius R via Eq. (7). We can then evaluate Eq. (8) to obtain the rate of change of $n(R, t_0)$ and determine $n(R, t_0 + dt)$ at an incremented time. By iterating this process, we can integrate Eq. (8) in time using an Euler update scheme. This can be done for a given free energy function. In the following examples, we choose for simplicity a Ginzburg-Landau free energy of a ternary mixture, i.e., $f(c_A, c_B) = b(c_A^c + c_B^s + c_0)^2 (c_A^c + c_B^s - c_0)^2 / (8c_0^2) + b(c_B^c - c_A^s)^2 / 2$ where b is an energy scale, c_0 a reference concentration, and $c_i^c = \cos(\alpha)c_i$ and $c_i^s = \sin(\alpha)c_i$, thereby parameterizing the interactions between components by a compositional angle α [36]; see the Appendix for further details.

In Figs. 2(a,d), we show two cases of the time evolution of the droplet size distribution as a function of the droplet radius R for different values of α , late times are shown in the insets. For both examples, Ψ_{tot} is chosen within the regime of extensive droplets, where single droplets grow without bounds [36], and the initial density distribution is Gaussian with N_0 droplets in a reference volume V_{ref} . In the first case, all droplets grow initially and reach a monodisperse steady state; see Fig. 2(c). We term this case arrested growth. In the second case, droplets exhibit ripening at early times, with smaller droplets shrinking while larger ones grow, thereby reducing the droplet number N (see Fig. 2(f)). At later times, the ripening stops, and a monodisperse stationary state of $N < N_0$ droplets is reached. We term this case arrested ripening. In both cases, the average droplet radius $\langle R \rangle$ grows initially and relaxes towards a constant value at large times; see Figs. 2(c),(f). This relaxation

to a monodisperse state can be explained as follows: As droplets grow by the influx of conserved material, the dilute phase concentration Ψ^∞ decreases. As a result, a stable droplet radius emerges for $\Psi^\infty < \psi_{\text{crit}}$. Once the average droplet radius $\langle R \rangle$ (indicated by dashed lines in Figs. 2(b,e)), which increases in time, meets the stable droplet radius, growth stops, and all droplets converge to the stable droplet radius. The result is a monodisperse emulsion. For comparison, in the case of Ostwald ripening of passive mixtures, the average droplet radius is always equal to the unstable droplet radius while no stable droplet radius exists, and the size distribution broadens.

Steady state - We can characterize the properties of the steady state of the active emulsion. If the number of droplets N is given, the size distribution is $n(R, \infty) = N\delta(R - R_s)$, where R_s denotes the stationary radius which obeys

$$\Psi_s^\infty = \Psi_R^o(R_s, \Psi_s^\infty). \quad (12)$$

This equation, together with the lever rule for the conserved quantity

$$\frac{4\pi R_s^3 N_s}{3V_{\text{ref}}} = \frac{\Psi_{\text{tot}} - \Psi_s^\infty}{\Psi_R^i(R_s, \Psi_s^\infty) - \Psi_s^\infty}, \quad (13)$$

determine the unknown values of R_s and Ψ_s^∞ . Note that this lever rule depends on the stationary droplet number N_s , in contrast to a passive system.

Scaling regime for late times - In passive mixtures, independently of the initial distribution, the size distribution widens and exhibits self-similarity at late times. There, $n(R, t) \propto g(x)(\tau/t)\langle R(t) \rangle^{-1}$, where τ is a time-scale and $g(x)$ is a universal distribution that depends on the dimensionless variable $x = R/\langle R(t) \rangle$ [43]. The average radius scales $\langle R(t) \rangle \propto t^{1/3}$, and consequently $N(t) \propto t^{-1}$ [6, 7]. In contrast, we find that in an active emulsion, the size distribution $n(R, t)$ at late times becomes narrow and centered around R_s . Droplets relax towards the stable radius R_s according to $\dot{R} = -\lambda(R - R_s)$, where $\lambda = -d\dot{R}/dR|_{R=R_s}$ using Eq. (7). This implies that the size distribution evolves as

$$n(R, t) = \frac{f(x)}{R_s} e^{\lambda t}, \quad x = \left(\frac{R - R_s}{R_s} \right) e^{\lambda t}, \quad (14)$$

where $f(x)$ is a time-independent function describing the shape. Indeed, Eq. (14) satisfies Eq. (8) in the long time limit for any normalizable function $f(x)$. Thus, $f(x)$ is not further constrained and depends on the initial distribution. Consequently, the droplet number is constant in time $N = \int_0^\infty dR n(R, t) = \int_0^\infty dx f(x)$.

To illustrate that the shape $f(x)$ of the size distribution depends on the initial distribution, we initialize the system presented in Figs. 2(a-c) with the same number of droplets N_0 but with sizes following the universal distribution $g(x)$ as an initial condition. Fig. 3(a) shows the droplet growth for this initial condition as well as

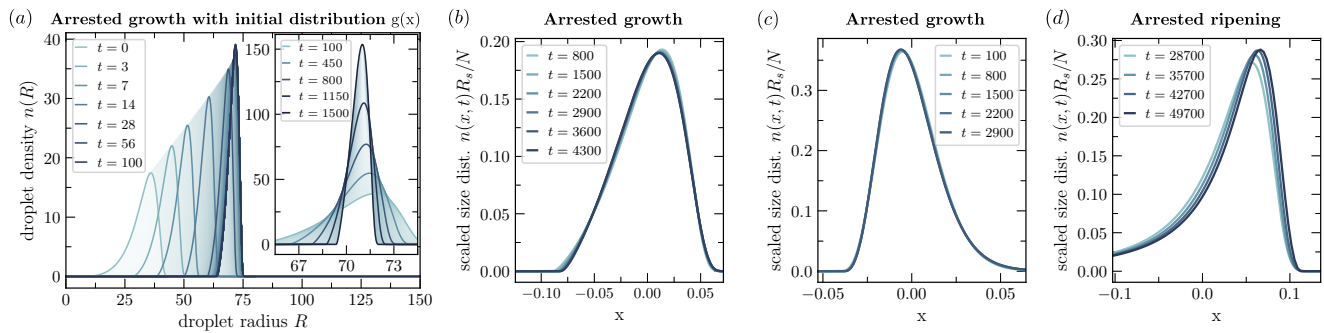


FIG. 3. **Shape of droplet size distributions at late times.** (a) Dynamics of the droplet size distribution $n(R)$ for the same system as shown in Fig. 2(a) but with an initial shape $g(x)$. The inset shows the distribution at late times. (b) Late time distribution as shown in (a) (inset), but scaled and shown as a function of scaled radius x . (c,d) Scaled plot as in (b) but showing late time distributions of arrested growth (Fig. 2(a)) and arrested ripening (Fig. 2(d)).

growth arrest at late times (inset). The rescaled curves nR_s/N as a function of scaled distance x for late times are shown in Fig. 3(b). For arrested growth, the total number of droplets is almost conserved. Thus, the stationary droplet size R_s and the relaxation rate λ are the same as for the previous case of arrested growth. To reveal this difference in the rescaled distributions, we show the scaled size distribution at different late times for arrested growth shown in Fig. 2(a) in Fig. 3(c). These scaled distributions converge to different shape functions $f(x)$ for late times; compare Fig. 3(b) and Fig. 3(c). Furthermore, we show the scaled distribution for arrested ripening, as shown in Fig. 2(d), in Fig. 3(d). Note that here, the shape function $f(x)$ of arrested ripening is similar to $g(x)$.

Finally, we comment on the effect of fluctuations on the droplet size distribution. In the simplest form, fluctuations can be accounted for by adding effective diffusion term with diffusivity \mathcal{D} to Eq. (8), writing $\partial_t n = \mathcal{D}\partial_R^2 n - \partial_R(n\dot{R})$. Expanding the interface velocity around the stationary radius, $\dot{R} = -\lambda(R - R_s)$, we obtain a Gaussian stationary distribution $n(R) = N\sqrt{\lambda/(2\pi\mathcal{D})}\exp[-\lambda(R - R_s)^2/(2\mathcal{D})]$. Recently, it was shown that the size distribution of condensates driven by active chemical processes in the nucleolus of living cells, i.e., the nucleolar fibrillar center, is well matched by a Gaussian in the regime of arrested ripening [44], consistently with our theory.

Discussion - In this work, we show how droplet size distributions emerge over time in chemically active emulsions, where droplets are coupled by conservation laws. In an active binary system without conservation law, droplets are only coupled locally [9]. Here, we have considered a minimal ternary system with a conserved density to investigate collective droplet dynamics in an active emulsion. This approach is similar to the theory developed for the passive ripening dynamics by Lifshitz, Slyosov, and Wagner [6, 7]. In the passive case, there is always a unique phase equilibrium that governs the ripening process. However, we show that in chemically

active emulsions, different phase equilibria are dynamically selected for different droplet sizes, which is evident in the size-dependence of the condition given in Eq. (6). Droplets grow when larger than the critical radius, consuming the conserved density in the far field. For sufficiently low far-field densities, there is a stable stationary droplet radius. The process arrests when droplets reach a stable size, leading to a monodisperse distribution. In contrast to passive emulsions, there is no unique stationary state. Indeed, the stationary state itself depends on the final droplet density N_s/V_{ref} (see Eq. (13)) and the late time distribution is not unique. However, the size distribution relaxes exponentially to a monodisperse distribution, keeping the shape of the size distribution invariant; see Eq. (14). Thus, our work shows that there is a universal scaling behavior in chemically active emulsions that leads to the collapse of the rescaled size distributions at late times (Fig. 3).

Our theory naturally generalized to more components and reactions, where the principles discussed here also apply. Our work could be applied to understand collective droplet dynamics in various experimental systems, such as biological condensates [44, 45] or engineered active emulsions in synthetic chemistry [46, 47]. Several questions remain open in such active droplet systems, including the role of fluctuations, effects of droplet division, shape instabilities, and nucleation. Integrating these and other aspects into our theory remains a challenge for future work.

Acknowledgment - J.B. thanks A. Goychuk for an insightful discussion and the German Research Foundation for financial support through the DFG Project BA 8210/1-1. G. B. thanks the Agencia Estatal de Investigación for funding through the Juan de la Cierva post-doctoral programme JDC2023-051554-I.

- * jbauer@fas.harvard.edu
† julicher@pks.mpg.de
- [1] W. Ostwald, *Zeitschrift für Physikalische Chemie* **22U**, 289 (1897).
 - [2] P. W. Voorhees, *Journal of Statistical Physics* **38**, 231 (1985).
 - [3] T. Pollock and A. Argon, *Acta metallurgica et materialia* **42**, 1859 (1994).
 - [4] J. Bibette, F. L. Calderon, and P. Poulin, *Reports on Progress in Physics* **62**, 969 (1999).
 - [5] L. Ratke and P. W. Voorhees, *Growth and Coarsening: Ostwald Ripening in Materials Processing*, Engineering Materials (Springer, Berlin Heidelberg, 2002).
 - [6] C. Wagner, *Zeitschrift für Elektrochemie, Berichte der Bunsengesellschaft für physikalische Chemie* **65**, 581 (1961).
 - [7] I. Lifshitz and V. Slyozov, *Journal of Physics and Chemistry of Solids* **19**, 35 (1961).
 - [8] S. C. Glotzer, D. Stauffer, and N. Jan, *Physical Review Letters* **72**, 4109 (1994).
 - [9] D. Zwicker, A. A. Hyman, and F. Jülicher, *Physical Review E* **92**, 012317 (2015).
 - [10] E. Tjhung, C. Nardini, and M. E. Cates, *Physical Review X* **8**, 031080 (2018).
 - [11] J. D. Wurtz and C. F. Lee, *Physical Review Letters* **120**, 078102 (2018).
 - [12] R. Singh and M. E. Cates, *Phys. Rev. Lett.* **123**, 148005 (2019).
 - [13] M. E. Cates and C. Nardini, arXiv:2412.02854 (2024).
 - [14] C. F. Lee and J. D. Wurtz, *Journal of Physics D: Applied Physics* **52**, 023001 (2018).
 - [15] C. A. Weber, D. Zwicker, F. Jülicher, and C. F. Lee, *Reports on Progress in Physics* **82**, 064601 (2019).
 - [16] D. Zwicker, arXiv preprint arXiv:2407.09859 (2024), arXiv:2407.09859 [cond-mat.soft].
 - [17] F. Jülicher and C. A. Weber, *Annual Review of Condensed Matter Physics* **15**, 237 (2024).
 - [18] A. A. Hyman, C. A. Weber, and F. Jülicher, *Annual Review of Cell and Developmental Biology* **30**, 39 (2014).
 - [19] Y. Shin and C. P. Brangwynne, *Science* **357**, eaaf4382 (2017).
 - [20] S. F. Banani, H. O. Lee, A. A. Hyman, and M. K. Rosen, *Nature Reviews Molecular Cell Biology* **18**, 285 (2017).
 - [21] S. Boeynaems, S. Alberti, N. L. Fawzi, T. Mittag, M. Polymenidou, F. Rousseau, J. Schymkowitz, J. Shorter, B. Wolozin, L. Van Den Bosch, P. Tompa, and M. Fuxreiter, *Trends in Cell Biology* **28**, 420 (2018).
 - [22] K. K. Nakashima, M. A. Vibhute, and E. Spruijt, *Frontiers in Molecular Biosciences* **6**, 21 (2019).
 - [23] C. A. Strulson, R. C. Molden, C. D. Keating, and P. C. Bevilacqua, *Nature Chemistry* **4**, 941 (2012).
 - [24] B. Drobot, J. M. Iglesias-Artola, K. Le Vay, V. Mayr, M. Kar, M. Kreysing, H. Mutschler, and T.-Y. D. Tang, *Nature Communications* **9**, 3643 (2018).
 - [25] C. Donau, F. Späth, M. Sosson, B. A. K. Kriebisch, F. Schnitter, M. Tena-Solsona, H.-S. Kang, E. Salibi, M. Sattler, H. Mutschler, and J. Boekhoven, *Nature Communications* **11**, 5167 (2020).
 - [26] P. S. Schwarz, S. Laha, J. Janssen, T. Huss, J. Boekhoven, and C. A. Weber, *Chemical Science* **12**, 7554 (2021).
 - [27] J. Heckel, F. Batti, R. T. Mathers, and A. Walther, *Soft Matter* **17**, 5401 (2021).
 - [28] C. Donau, F. Späth, M. Stasi, A. M. Bergmann, and J. Boekhoven, *Angewandte Chemie* **134**, e202211905 (2022).
 - [29] J. Kirschbaum and D. Zwicker, *Journal of The Royal Society Interface* **18**, 20210255 (2021).
 - [30] J. Bauermann, C. A. Weber, and F. Jülicher, *Annalen der Physik* **534**, 2200132 (2022).
 - [31] A. Kumar and S. A. Safran, *Physical Review Letters* **131**, 258401 (2023).
 - [32] Y. Cho and W. M. Jacobs, *The Journal of Chemical Physics* **159**, 154101 (2023).
 - [33] L. Demarchi, A. Goychuk, I. Maryshev, and E. Frey, *Physical Review Letters* **130**, 128401 (2023).
 - [34] G. Häfner and M. Müller, *ACS nano* (2024).
 - [35] A. Shelest, H. Le Roy, D. M. Busiello, and P. De Los Rios, *The Journal of Chemical Physics* **162** (2025).
 - [36] J. Bauermann, G. Bartolucci, J. Boekhoven, F. Jülicher, and C. A. Weber, arXiv preprint arXiv:2409.03629 (2024), arXiv:2409.03629 [cond-mat.soft].
 - [37] P. W. Voorhees, *Annual Review of Materials Science* **22**, 197 (1992).
 - [38] J. H. Yao, K. R. Elder, H. Guo, and M. Grant, *Phys. Rev. B* **47**, 14110 (1993).
 - [39] J. Bauermann, S. Laha, P. M. McCall, F. Jülicher, and C. A. Weber, *Journal of the American Chemical Society* **144**, 19294 (2022).
 - [40] S. Safran, *Statistical Thermodynamics of Surfaces, Interfaces, and Membranes*, first issued in hardback ed., *Frontiers in Physics* No. 90 (CRC Press, Taylor & Francis Group, Boca Raton London New York, 2019).
 - [41] C. J. Kuehmann and P. W. Voorhees, *Metallurgical and Materials Transactions A* **27**, 937 (1996).
 - [42] A. Bray, *Advances in Physics* **43**, 357 (1994).
 - [43] $g(x) = x^2(3+x)^{-7/3}(3/2-x)^{-11/3} \exp(-x/(3/2-x))$.
 - [44] S. F. Banani, A. Goychuk, P. Natarajan, M. M. Zheng, G. Dall’Agnese, J. E. Henninger, M. Kardar, R. A. Young, and A. K. Chakraborty, bioRxiv (2024).
 - [45] S. Saurabh, T. N. Chong, C. Bayas, P. D. Dahlberg, H. N. Cartwright, W. E. Moerner, and L. Shapiro, *Science Advances* **8**, 10.1126/sciadv.abm6570 (2022).
 - [46] K. K. Nakashima, M. H. I. van Haren, A. A. M. André, I. Robu, and E. Spruijt, *Nature Communications* **12**, 10.1038/s41467-021-24111-x (2021).
 - [47] C. Donau, F. Späth, M. Stasi, A. M. Bergmann, and J. Boekhoven, *Angewandte Chemie International Edition* **61**, 10.1002/anie.202211905 (2022).

APPENDIX

Multicomponent Flory-Huggins model

We used a simple Flory-Huggins free energy density of a ternary mixture for generating Fig. 1. This free energy is typically written in terms of the volume fractions ϕ_A , ϕ_B and ϕ_S , i.e., the fraction of space occupied by particles of type A , B and S , such that $\phi_A + \phi_B + \phi_S = 1$. In its simplest form, it reads

$$f(\phi_A, \phi_B) = \frac{k_B T}{\nu} \left(\sum_{i=A,B,S} \phi_i \log(\phi_i) + \sum_{i,j=A,B,S} \chi_{ij} \phi_i \phi_j + \sum_{i=A,B,S} w_i \phi_i \right), \quad (15)$$

where $k_B T$ sets the energy scale and ν is a reference volume of the molecules. The first sum accounts for the entropic contribution of mixing. The second sum represents an energy contribution coming from the interaction between components i, j . Here, χ_{ij} is a dimensionless interaction strength. Furthermore, it is sufficient to take only the pairs $(i, j) = (A, B), (A, S), (B, S)$ into account. The last sum represents the internal energy contribution of molecules of type i , where w_i is a dimensionless weight factor.

In the figure, we have chosen $\chi_{AB} = 0$, $\chi_{AS} = 3.2$, $\chi_{BS} = 0.4$, $w_A = w_S = 0$, $w_B = 1.8$, while the energy scale $k_B T$ and the reference volume ν do not affect the shape of the phase diagram at thermodynamical equilibrium. However, for finite-sized droplets and their \dot{R} -curves, we have to specify the surface tension γ : we have chosen $\gamma\beta\nu = \ell/6$, where ℓ is our reference length-scale, related to the interface width and sometimes called capillary width. In addition, we give all time scales in terms of τ , the time it takes for a particle to diffuse across an area of ℓ^2 . Consequently, we set $D = 1\ell^2/\tau$. For the passive system, the chemical reaction finds its equilibrium fast and only the conserved quantity has to be taken into account. Therefore, to obtain the interface velocities, we have to replace Eq. (6) with the condition $\mu_A^{i/o} = \mu_B^{i/o}$. The reaction rates, however, do not matter. For the active setting, however, we have to specify the rates. We set $k_{AB} = 0.001\tau^{-1}$ and $k_{BA} = 0.0006\tau^{-1}$, such that $k_{BA}/k_{AB} = 1/6$, the slope of the reaction nulcline in the phase diagram.

Generic form of the free energy with simple phase equilibria

Fig. 1 in the main text shows the \dot{R} , which is the key ingredient of the theory obtained from a Florry-Huggins free energy model, demonstrating that the theory proposed in the main text can be applied, in principle, to many classical problems studied in the literature. For such systems, however, the interface conditions (i.e., Eq. (5)) lead to non-algebraic constraints that must be found numerically. To simplify the analytics for the remaining figures and results, we have chosen a simpler free energy density combining a bi-quadratic and a quadratic term, i.e.,

$$f(c_A, c_B; \alpha) = \frac{b}{8c_0^2} (\cos(\alpha)c_A + \sin(\alpha)c_B + c_0)^2 (\cos(\alpha)c_A + \sin(\alpha)c_B - c_0)^2 + \frac{b}{2} (\cos(\alpha)c_B - \sin(\alpha)c_A)^2, \quad (16)$$

where b is a scale of the free energy density. For $\alpha = 0$, the first term leads to a Cahn-Hilliard dynamics for A with the equilibrium concentrations $\pm c_0$, while B diffuses freely in and between the phases. Whenever $\alpha \neq 0$, molecular interactions rotate this simple free energy. For further details, see [36].

We can find the four equilibrium concentrations $\Psi^{i/o}$ and $\Xi^{i/o}$ analytically. Three conditions follow from the assumption of local phase equilibrium, i.e., Eq. (5), while Eq. (6) determines then uniquely one phase equilibrium as a function of R and ψ^∞ . The Laplace pressure in Eq. (5) ($\propto 2\gamma/R$), leads to a finite size correction of the equilibrium concentrations. By using a so-called Gibbs-Thomson coefficient β , we can approximate to linear order

$$\Psi^{i/o} = \Psi_0^{i/o} + 2\beta\gamma(\cos(\alpha) + \sin(\alpha))/R, \quad \Xi^{i/o} = \Xi_0^{i/o} + 2\beta\gamma(\cos(\alpha) - \sin(\alpha))/R, \quad (17)$$

where $\Psi_0^{i/o}$ and $\Xi_0^{i/o}$ are the equilibrium values of an infinite big system. These boundary conditions, together with Eq. (6), determine uniquely the phase equilibrium of a droplet of size R . The phase equilibria of the conserved

quantity on both sides at the interface read

$$\begin{aligned} \Psi^i(R, \psi^\infty) = & \left(k\psi^\infty + \lambda(4\beta\gamma k - c_0 R(k+s)) \cos(\alpha) - \psi^\infty s \cos(2\alpha) + \lambda c_0 R(k-s) \cos(3\alpha) - 2(k\lambda(c_0 R - 2\beta\gamma) \right. \\ & \left. + k\psi^\infty \cos(\alpha) + \lambda c_0 R(k+s) \cos(2\alpha)) \sin(\alpha) + 2k\lambda(2\beta\gamma - c_0 R) \coth(\lambda R)(\cos(\alpha) + \sin(\alpha)) \right) \\ & / \left(k + k\lambda R + (\lambda R - 1)s \cos(2\alpha) + k(\lambda R - 1) \sin(2\alpha) + \lambda R \coth(\lambda R)(k + s \cos(2\alpha) + k \sin(2\alpha)) \right) \end{aligned} \quad (18)$$

$$\begin{aligned} \Psi^o(R, \psi^\infty) = & \left(k\psi^\infty + (4\beta\gamma k\lambda + (k + 2k\lambda R - s)c_0) \cos(\alpha) - \psi^\infty s \cos(2\alpha) + (k-s)c_0 \cos(3\alpha) \right. \\ & \left. - 2(-k\lambda(2\beta\gamma + Rc_0) + k\psi^\infty \cos(\alpha) + (k+s)c_0 \cos(2\alpha)) \sin(\alpha) + 2\lambda \coth(\lambda R)(\cos(\alpha) + \sin(\alpha)) \right. \\ & \left. \times (2\beta\gamma k + Rsc_0 \cos(2\alpha) + kRc_0 \sin(2\alpha)) \right) / \left(k + k\lambda R + (\lambda R - 1)s \cos(2\alpha) + k(\lambda R - 1) \sin(2\alpha) \right. \\ & \left. + \lambda R \coth(\lambda R)(k + s \cos(2\alpha) + k \sin(2\alpha)) \right), \end{aligned} \quad (19)$$

where $\lambda = \sqrt{k/D}$. Here, for simplicity, we have assumed $D_\psi^i = D_\psi^o = D_\xi^i = D_\xi^o = D$, $k^i = k^o = k$, $s^i = s^o = s$. With these solution and Eq. (11), we find

$$\begin{aligned} \psi^\infty(\langle R \rangle, \phi) = & \left(-k\Psi_{\text{tot}}(1 + \lambda\langle R \rangle) + \lambda\phi(4\beta\gamma k - \langle R \rangle(k+s)c_0) \cos(\alpha) + \Psi_{\text{tot}}(1 - \lambda\langle R \rangle)s \cos(2\alpha) + \lambda\phi\langle R \rangle(k-s)c_0 \cos(3\alpha) \right. \\ & \left. + \lambda\phi(4\beta\gamma k + \langle R \rangle(s-k)c_0) \sin(\alpha) - \lambda \coth(\lambda\langle R \rangle)(\cos(\alpha) + \sin(\alpha))(2k\phi(-2\beta\gamma + \langle R \rangle)c_0) \right. \\ & \left. + \Psi_{\text{tot}}\langle R \rangle(k+s) \cos(\alpha) + \Psi_{\text{tot}}\langle R \rangle(k-s) \sin(\alpha) + k\Psi_{\text{tot}}(1 - \lambda\langle R \rangle) \sin(2\alpha) - \lambda\phi\langle R \rangle(k+s)c_0 \sin(3\alpha) \right) \\ & / \left((1 + \lambda(\phi - 1)\langle R \rangle)s \cos(2\alpha) + \lambda(\phi - 1)\langle R \rangle \coth(\lambda\langle R \rangle)(k + s \cos(2\alpha) + k \sin(2\alpha)) \right) \end{aligned} \quad (20)$$

$$+ k(-1 + \lambda(\phi - 1)\langle R \rangle + (1 + \lambda(\phi - 1)\langle R \rangle) \sin(2\alpha)), \quad (21)$$

where Ψ_{tot} is the concentration of the conserved density in the system. With the equations above, we have explicit conditions for the boundary conditions and the closed set of dynamical equations, as described in the main text, can be iterated straightforwardly.